Asian Journal of Chemistry; Vol. 27, No. 7 (2015), 2678-2684

ASIAN JOURNAL OF CHEMISTRY

http://dx.doi.org/10.14233/ajchem.2015.18839

Raman Spectra, Molecular Modeling and Biological Studies on Buffering Agent Metal Complexes

FAWAZ SAAD[1], KHLOOD S. ABOU-MELHA[2] and NASHWA M. EL-METWALY[1,3,*]

[1]Chemistry Department, Faculty of Applied Science, Umm Al-Qura University, Makah, Saudi Arabia
[2]Chemistry Department, Faculty of Science of Girls, King Khalid University, Saudi Arabia
[3]Chemistry Department, Faculty of Science, Mansoura University, Mansoura, Egypt

*Corresponding author: Tel: +966 55 3205965; E-mail: n_elmetwaly00@yahoo.com

Received: 5 November 2014; *Accepted*: 13 December 2014; *Published online*: 30 March 2015; AJC-17105

Some transition metal complexes was prepared using a trizma buffering agent as a coordinating ligand. A slim organic compound used, produces a simple complexes serve in biological application. The complexes are investigated through elemental, thermal, spectral and molecular modeling. The general coordination binding mode of the ligand is the bidentate binding through a mononegative with Mn(II) and Cr(III) complexes, or neutral with Fe(III), Zn(II) and Cd(II) ions. The octahedral bonding distribution are proposed for all investigated metal complexes. The molecular modeling calculations reflect a shadow on comparative stability in between metal complexes. The biological investigation was concerned with the inhibition activity towards some bacteria as well as the degradation of DNA. Cadmium(II) complex displays the most insecticidal activity towards all used microorganisms. Also, all the complexes display a distinguish behavior towards DNA.

Keywords: Trizma complexes, Raman, DNA degradation, Molecular modeling.

INTRODUCTION

tris(2,3-Dibromopropyl) phosphate, has been reported to be a cancer suspect agent. Trizma and its salts have been useful as buffers in a wide variety of biological systems. Its uses include pH control *in vitro*[1,2] and *in vivo*[3,4] for body fluids and as an alkalizing agent in the treatment of acidosis of the blood[5]. Trizma has been used as a starting material for polymers, oxazolones (with carboxylic acids) and oxazolidines (with aldehydes)[6]. Trizma does not precipitate calcium salts and is of value in maintaining solubility of manganese salts[7]. Trizma base and trizma HCl are both available in Tissue culture, plant tissue culture. The interaction of DNA with transition metal complexes has attracted a considerable interest due to its various applications in cancer therapy and molecular biology[8-14]. Class of compounds, when compared to existing bactericidal drugs, shows improved pharmacokinetic properties and a broad spectrum of activity against parasites, bacteria and mycobacterium, including resistant strains. In addition to that they displayed significant *in vitro* antibacterial activity against many Gram-positive and Gram-negative bacteria through inhibition of their DNA gyrase[15]. Hydrolytic cleavage of double stranded DNA involving phosphodiester bond offers important advantages in the cellular processes in comparison to the oxidative DNA cleavage targeted at the deoxyribose sugar moiety or the guanine base[16-19]. The aim of this work is the preparation of some complexes derived from slim buffering agent (trizma). The preparation of trizma - transition metal ion complexes are completely absent in the literature. These little crowded complexes may serve by a distinguish way in the biological field especially with the DNA degradation. The metal ions used were chosen deliberately based on their biological history. Also, the molecular modeling investigation offer a good view about the stability of the proposed structures which may affect directly on the attach with DNA.

EXPERIMENTAL

All chemicals used for the study were of analytically reagent grade, commercially available from Fulka and used without previous purification *e.g.*, trizma[2-amino-2-(hydroxymethyl)propane-1,3-diol], $CrCl_3 \cdot 6H_2O$, $MnCl_2 \cdot 4H_2O$, $FeCl_3 \cdot 6H_2O$, $ZnCl_2$ and $CdCl_2$.

Synthesis of metal complexes: All the metal complexes were prepared by heating 1:2 molar ratio from 2-amino-2-(hydroxymethyl)propane-1,3-diol (H_3AHMP) (trizma) (0.485 g, 4 mmol) with corresponding metal chloride salt in ethanolic medium. The reaction medium was adjusted using few drops of NH_4OH till pH = 6-7 and then heated in a water bath for 1-2 h under reflux. The precipitate was filtered off washed with ethanol, diethyl ether and finally dried in a vacuum desiccators.

Antimicrobial activity: The ligand and its metal complexes were screened for their antimicrobial activity using the cup-diffusion technique[20] against *Bacillus* sp. as gram positive and *Klebsiella* sp. and *Proteus* sp. as gram negative bacteria. A 0.2 ml of a tested substance (10 µg/mL) was placed in specified cup made in the nutrient agar medium on which a culture of the tested bacteria has been spread to produce uniform growth. After 24 h incubation at 37 °C, the diameter of inhibition zone was measured as mm.

Genotoxicity: A solution of Calf thymus DNA (2 mg) was dissolved in 1 mL of sterile distilled water to a final concentration of 2 g/L. Stock concentrations of the ligand and metal complexes were prepared by dissolving 2 mg/mL in DMSO. An equal volume of each compound and DNA were mixed thoroughly and kept at room temperature for 2-3 h. The effects of the chemicals on DNA were analyzed by agarose gel electrophoresis. A 2 µL of loading dye was added to 15 µL of the DNA-chemical mixture before being loaded into the wall of an agarose gel. The loaded DNA-chemical mixtures were fractionated by electrophoresis, visualized by UV and photographed.

Physical measurements: Carbon and H were analyzed at the microanalytical unit. Mn(II), Zn(II), Cd(II), Fe(III) and Cr(III) were determined by complexometric titration methods[21], whereas, the conjugated anion was determined gravimetrically[21]. The molar conductivities of freshly prepared 1×10^{-3} mol/cm^3 DMSO solutions were measured for complexes using Jenway 4010 conductivity meter. The infrared spectra, as KBr discs, were recorded on a Mattson 5000 FTIR Spectrophotometer (4000-400 cm^{-1}). The electronic and ^{1}H NMR (200 MHz) spectra were recorded on UV_2 Unicam UV-visible and a Varian Gemini Spectrophotometers, respectively. The effective magnetic moments were evaluated at room temperature by applying $\mu_{eff} = 2.828\sqrt{\chi_M T}$, where χ_M is the magnetic susceptibility corrected using Pascal's constants for the diamagnetism of all atoms in the ligand using a Johnson Matthey magnetic susceptibility balance. The thermal studies were carried out on a Shimadzu thermogravimetric analyzer (20-800 °C) at a heating rate of 10 °C min^{-1} under nitrogen. Raman laser spectra of samples were measured on the Bruker FT- Raman with laser 50 mW. The biological study was carried out in Molecular Biology Center, Botany Department.

Molecular modeling: An attempt to obtain an acceptable insight about the molecular modeling structure of the ligand (Fig. 1) and its metal complexes was done. The geometry optimization and conformational analysis has been performed in Table-5 by the use of MM$^+$ force-field[22] as implemented in hyperchem 5.1[23].

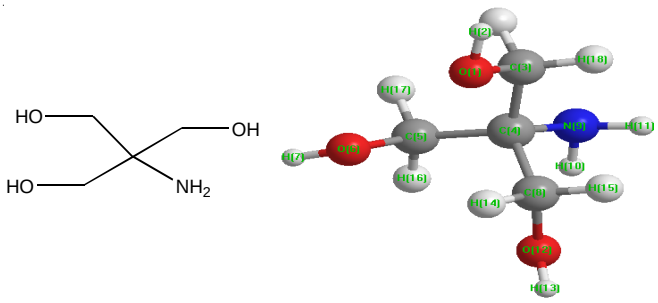

Fig. 1. Structure and the molecular modeling of Trizma (H_3AHMP) [2-amino-2-(hydroxymethyl)propane-1,3 diol]

RESULTS AND DISCUSSION

The elemental analysis data are displayed in Table-1, as well as the conductivity measurements. The measurements reveal the non conducting feature for all investigated complexes except $[FeCl(C_4H_{11}NO_3)_2(H_2O)]\cdot 2Cl$ and $[Cd(C_4H_{11}NO_3)_2(H_2O)]\cdot 2Cl$ complexes.

IR spectra and mode of bonding: A comparison for the significant band position in between the free ligand and its metal complexes will give enough insight to the way of its bonding towards the metal ions. The spectra were carried in the range of 4000-400 cm^{-1} and the most significant bands are listed in Table-2. The spectrum of the ligand displays a series of significant bands[24] as: 3352, 3291, 3196, 1590 and 1397 cm^{-1} which may be assigned to νOH, $\nu_{as}NH_2$, ν_sNH_2, δNH and δOH in plane. The stretching and bending bands of OH and NH groups suffer a lower appearance. This may propose the presence of intraligand H - bonding in between the neighboring groups. Trizma ligand bonded towards all metal ions [Cr(III), Mn(II), Fe(III), Cd(II) and Zn(II)] by the same mode of coordination through two active sites (NH_2 and OH) in neutral or monoanionic state. A mono negative bidentate coordination mode is appeared with each coordinating ligand in $[CrCl(C_4H_{10}NO_3)_2\cdot H_2O]\cdot 2H_2O$ and $[Mn(C_4H_{10}NO_3)_2\cdot 2H_2O]$ complexes. NH_2 group and enolized OH are the two chelating arms towards the Cr(III) ion. The lower shift observed obviously for $\nu_{as}NH_2$ and ν_sNH_2 bands and the appearance of new band at 1039 cm^{-1} assigned to ν(C-O), are supporting the former proposal. The reaction medium pH effects directly on the ligand coordination mode especially with such catalytically active metals. The appearance of ν(OH) and δ(OH) bands supports the presence of one or two groups without enolizaton. A neutral bidentate mode, is the second mode proposed with the other complexes as: $[FeCl(C_4H_{11}NO_3)_2\cdot 2H_2O]\cdot 2Cl$, $[ZnCl_2(C_4H_{11}NO_3)_2]$ and $[Cd(C_4H_{10}NO_3)_2\cdot 2H_2O]\cdot 2Cl$. Each ligand coordinates *via* NH_2 and OH groups. The lower shift appearance of their ν and δ bands, supports the former proposal. Their structural

TABLE-1
ANALYTICAL AND PHYSICAL DATA FOR TRISMA (H_3AHMP) LIGAND AND ITS METAL COMPLEXES

Compound	Colour	Λ_m	Elemental analysis (%) Calcd. (found)			
Empirical formula (m.w.)		(Ω^{-1} cm^2 mol^{-1})	C	H	M	Cl
$[C_4H_{11}NO_3]$ (H_3L) (121.14)	Yellow	-	-	-	-	-
$[CrCl(C_4H_{10}NO_3)_2(H_2O)]\cdot 2(H_2O)$ (381.76)	Green	22	25.17 (25.17)	6.86 (6.85)	13.62 (13.62)	9.29 (9.31)
$[Mn(C_4H_{10}NO_3)_2\cdot 2H_2O]$ (331.23)	Brown	19	29.00 (29.20)	7.30 (7.60)	16.58 (16.57)	-
$[FeCl(C_4H_{11}NO_3)_2(H_2O)]\cdot 2Cl$ (422.50)	Brown	105	22.74 (22.73)	5.72 (5.75)	13.22 (13.21)	25.17 (25.17)
$[ZnCl_2(C_4H_{11}NO_3)_2]$ (378.58)	White	15	25.38 (25.37)	5.86 (5.88)	17.27 (17.28)	18.73 (18.72)
$[Cd(C_4H_{11}NO_3)_2(H_2O)]\cdot 2Cl$ (461.63)	White	115	20.82 (21.02)	5.68 (5.66)	24.35 (24.34)	15.36 (15.36)

TABLE-2
ASSIGNMENTS OF ESSENTIAL IR (RAMAN) SPECTRAL BANDS (cm^{-1}) OF H_3AHMP AND ITS METAL COMPLEXES

Compound	ν(OH)	$\nu_{as}(NH_2)$	$\nu_s(NH_2)$	ν(C-O)	δ(OH) in plane	$\delta(NH_2)$	δ(OH) out of plane	ν(M-Cl)	ν(M-N)	ν(M-O)	ν(M-OH_2)
$[C_4H_{11}NO_3]$ (H_3L)	3352	3291	3196	1029	1397	1590	629	-	-	-	
	(3341)	-	-	(1069)	(1340)	(1500)	(750)	-	-	-	
$[CrCl(C_4H_{10}NO_3)_2(H_2O)]\cdot 2(H_2O)$	3190	3108	2990	1039	1401	1551	662	-	524	594	906
	(3180)	-	-	(1038)	(1340)	(1600)	(650)	(260)	(470)	(580)	(905)
$[Mn(C_4H_{10}NO_3)_2\cdot 2H_2O]$	3227	3160	3106	1039	1401	1552	662	-	524	594	906
	(3350)	(3150)	-	(1040)	(1340)	(1580)	(650)	-	(350)	(520)	(905)
$[FeCl(C_4H_{11}NO_3)_2\cdot H_2O]\cdot 2Cl$	3227	3160	3106	1039	1297	1629	663	-	450	594	-
$[ZnCl_2(C_4H_{11}NO_3)]$	3528	3262	3224	1038	1344	1591	641	-	419	497	-
	(3400)	(3175)	-	(1050)	(1370)	(1650)	(710)	(230)	(460)	(490)	
$[Cd(C_4H_{11}NO_3)_2\ 2(H_2O)]\cdot 2Cl$	-	3229	-	1040	1298	1585	659	-	470	650	-

distribution primates the chelation of the two groups. This is supported by the data abstracted from the molecular modeling (MM^+) implementing hyperchem 5.1. The ruling out of the role of two function groups cannot detected clearly from the data. This is referring to the presence of intraligand H^- bonding. All over the spectra, new bands were appeared at lower frequency region (500-400 cm^{-1}) assigned for ν(M-N) and ν(M-O)[25]. While the ν(M-Cl) band cannot easily detected over a hall scanning range.

Resonance Raman: Resonance Raman spectra were carried out for all investigated compounds in their solid state. Such is a very useful technique to find out the oxidation state of the ligand because it is sensible to slight changes in the electron distribution over a hall molecule. Fig. 2, displays spectra of Zn(II), Cr(III) complexes and ligand. The spectra of Fe(III) and Cd(II) complexes were excluded due to a confusion prohibit the exact characterization. As can be seen, all the complexes show a very similar pattern. The significant spectral similarity among the trivalent and divalent metal complexes although the variable coordination mode in between the metal ions. Table-2 summarize the observed vibrational wave numbers aggregated with IR data. Resonance Raman spectra of Cr(III) and Mn(II) complexes show band profile characteristic for the compounds. The high wave number Raman peaks may be assigned to internal ligand vibrations at 3180 and 3350 cm^{-1} to O-H stretching, νOH in the two complexes, respectively. One of the most intense band observed at 1600 and 1580 cm^{-1}, in the two complexes, respectively is a very characteristic for N-H deformation. The other intense band at 1370 or 1340 cm^{-1} is characteristic for O-H deformation, in plane. The band observed at 1038 and 1040 cm^{-1} for the two complexes, respectively, assigned to ν(C-O)[26]. The resonance spectrum of Zn(II) complex shows bands profile characteristic for the compound. The high wave number Raman peaks at 3400 and 3175 cm^{-1} assigned to νOH and $\nu_{as}NH_2$, respectively. The bands at 1650, 1370 and 1050 cm^{-1} assigned for δNH, δOH and νC-O. The bands are shifted towards higher wave numbers in comparing with free ligand and slightly decreases in the series Zn(II) → Cr(III) → Mn(II). The higher intensity of the bands may be proposed the presence of trizma as bi nucleus in the same complex. In the spectrum of Zn(II)–trizma most of the studied bands undergo displacement towards higher wave numbers in comparing to the others. The metal ions influence the electronic charge distribution to a small extend, on the basis of the magnitude of bands shifts from spectra we

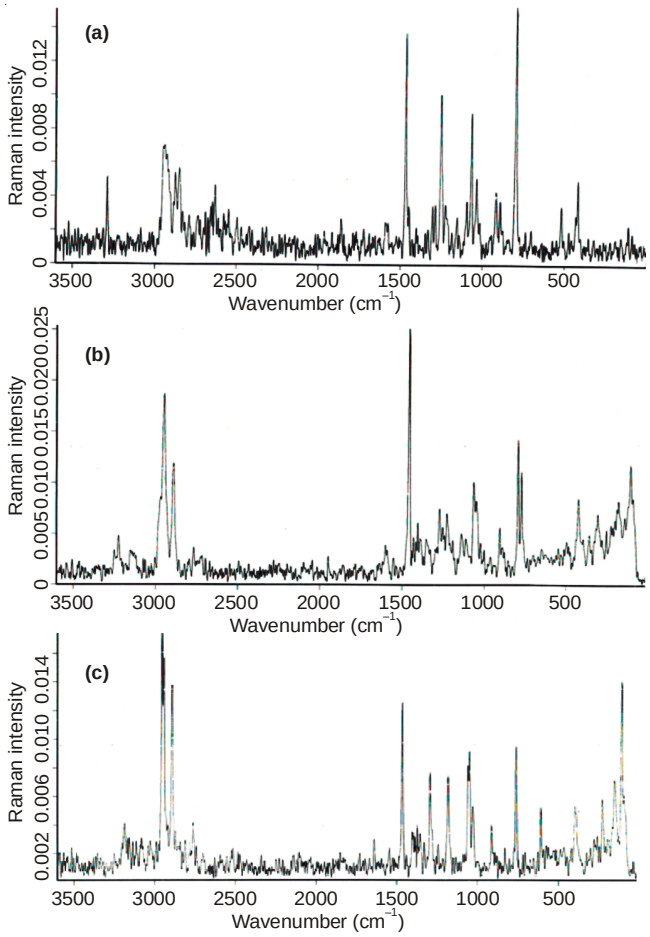

Fig. 2. Raman spectra of, trizma (A); Zn(II) complex (B); Cr(III) complex (C)

may conclude that the Zn(II) complex among the studied others shows the highest stability. The low frequency spectral region gives important information about the nature of the metal-ligand bonds. Bands around 600 and 400 cm^{-1} in all complexes spectra were observed and assigned to ν(M-O) and ν(M-N), vibrations, respectively[27]. The band doesn't present in intense state but just weak bands. Finally, the other significant low intense band at 260 and 230 cm^{-1} are assigned to ν(M-Cl) terminal bond in Cr(III) and Zn(II) complexes, respectively, which cannot be detected from the used IR spectral range.

^{1}H NMR spectral studies: ^{1}H NMR spectra in DMSO-d_6 are carried out for the ligand and two of its metal complexes. The spectrum of the ligand showed the following essential peaks; δ = 2 for alcoholic (3OH) protons and δ = 2.2 for NH_2

protons. ^{1}H NMR spectra of Cd(II) and Zn(II) complexes are displaying significant peaks as fellow: Cd(II) complex spectrum, δ = 4.27 for CH_2 protons, δ = 3.33 for H_2O + DMSO, δ = 3.09 and 2.50 for 6OH and $2NH_2$ protons, respectively. Zn(II) complex spectrum, δ = 4.23 for CH_2 protons, δ = 3.36 for DMSO, δ = 3.12 and 2.49 for 6OH and $2NH_2$ protons, respectively. The downfield appearance of all function groups reflects the participation of some of them and the presence of intraligand H- bonding in between others.

Magnetic susceptibility and electronic spectral measurements: The magnetic susceptibility value and the d-d transition bands are coincide with each other to propose the stereo structural arrangment around the central metal ions (Fig. 3). The magnetic moment values and the significant transition bands for all complexes in solution state (using DMF) are located in Table-3. The absorption spectrum of $[CrCl(C_4H_{10}NO_3)_2 \cdot H_2O] \cdot 2H_2O$ complex reveals significant bands at 17,666 and 24,876 assigned for $^4A_2g(F) \rightarrow {}^4T_2g(F)(\nu_1)$ and $^4A_2g(F) \rightarrow {}^4T_1g(F)$ (ν_2) *d-d* transitions, respectively. These bands characteristics for octahedral geometry around Cr(III) ion[28]. The μ_{eff} value of the Cr(III) complex has been reported as 4.50 BM, which is coincide with the geometry proposed for high spin state of the isolated complex. The absorption spectrum of $[Mn(C_4H_{10}NO_3)_2 \cdot 2H_2O]$ complex shows bands at 18,182 and 23,923 cm^{-1} assigned to $^6A_1g \rightarrow {}^4T1g(^4G)$ and $^6A_1g \rightarrow {}^4T_2g(^4G)$ transitions, respectively. This completely agrees with high spin octahedral as well as, the μ_{eff} value (5.36 BM) are in a parallel with the spectral data[29]. The $[FeCl(C_4H_{11}NO_3)_2 \cdot 2H_2O] \cdot 2Cl$ spectrum displays band at 20,833 assigned to $^6A_1g \rightarrow {}^4T_2g(G)$ transition in octahedral geometry around the central atom. The magnetic moment value (6.70 BM) is considered the further support for the proposed structure. Zn(II) and Cd(II) d^{10} systems, the charge transfer bands are the only appeared in the spectra and did not reflect any about the stereo structure of the complexes. Whereas, the structure proposed based on the electronic configuration of the two metal ions. The octahedral structure is the main stereo expected for the two complexes.

Thermal analysis and kinetics: The decomposition stages, temperature ranges, proposed decomposition products as well as the calculated and found weight loss percentages of the complexes are presented in Table-4. In $[CrCl(C_4H_{10}NO_3)_2 \cdot H_2O] \cdot 2H_2O$ complex, the TG and DTG curves show three decomposition stages started at 40.9 °C and ended at 800 °C. The complex reveals a lower thermal stability up to 40 °C and followed by a sudden decomposition by a weight loss 4.20 (calcd. 4.72 %) which corresponding to the elimination of hydrated H_2O molecule. The second endothermic decomposition stage ended at 443.1 °C corresponding to the removal of L + $2H_2O$ by 40.1 (calcd. 40.91 %) weight loss. The third degradation stage ended at 800 °C corresponding to $0.5Cl_2$ + (L-O) by 37.6 (calcd. 36.83 %) weight loss. The final residue recorded at 800 °C attributed to CrO. The TG curves display three gradual degradation stages for $[Mn(C_4H_{10}NO_3)_2 \cdot 2H_2O]$ complex started at 155.9 °C and ended at 616.1 °C. The first degradation stage ended at 313.3 °C is attributed to the fast degradation for H_2O + L by 47 (calcd. 47.12 %) weight loss. The second degradation stage ended at 441.3 °C is attributing to the removal of CO + H_2 as a small fragment by 9.10 (calcd.

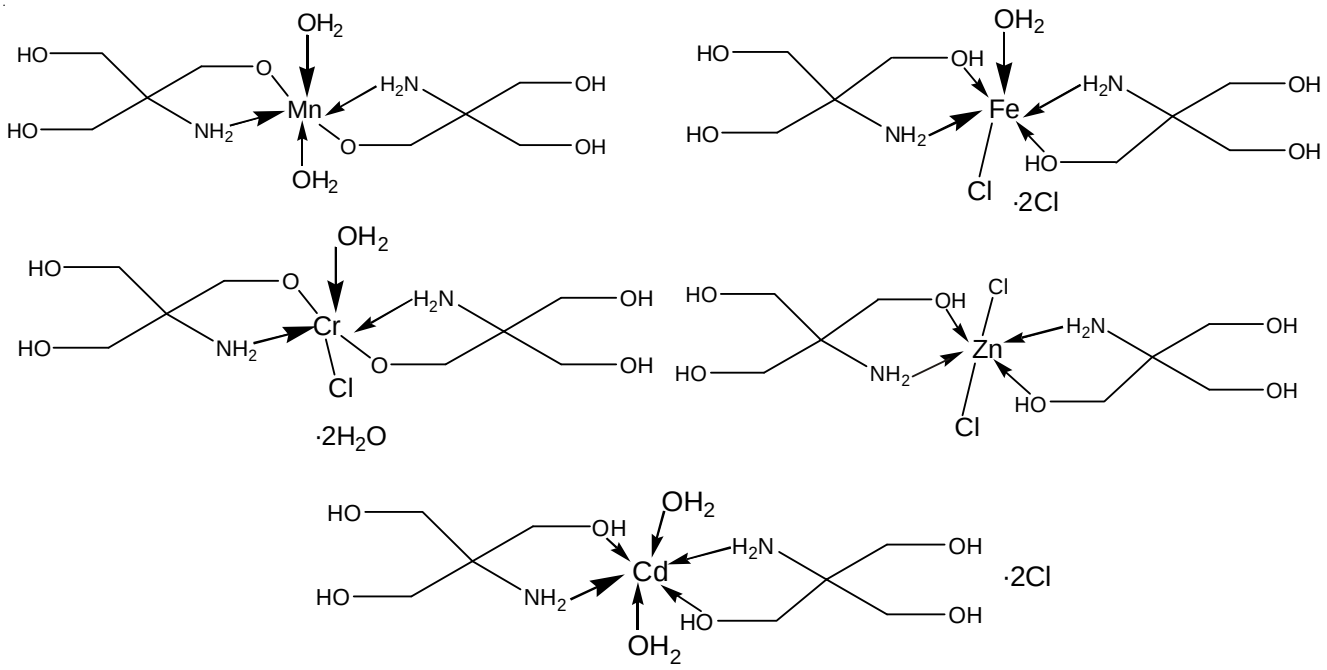

Fig. 3. Proposed stereo structure for all investigated metal complexes

TABLE-3
MAGNETIC MOMENTS (BM) AND ELECTRONIC SPECTRAL BANDS (cm^{-1}) OF SOME METAL COMPLEXES

Complex	μ_{eff} (BM)	*d-d* Transition (cm^{-1})	Intra-ligand and charge transfer (cm^{-1})
$[CrCl(C_4H_{10}NO_3)_2 \cdot (H_2O)] \cdot 2(H_2O)$	4.50	17,666; 24,876	39,682; 36,231; 33,113
$[Mn(C_4H_{10}NO_3)_2 \cdot 2H_2O]$	5.36	18,182; 23,923	37,313; 31,250
$[FeCl(C_4H_{11}NO_3)_2 \cdot H_2O] \cdot 2Cl$	6.70	20,833	43,103; 34,965; 27,472

TABLE-4
THERMOGRAVIMETRIC ANALYSIS DATA OF THE INVESTIGATED METAL COMPLEXES

Complex	Steps	Temperature range (°C)	Decomposed assignments	Weight loss found (Calcd. %)
(2)	1st	40.9- 97.1	-H_2O	4.20 (4.72)
	2nd	211.1-443.1	-L + 2 H_2O	40.1 (40.91)
	3rd	443.1-800	-0.5 Cl_2 + (L-O)	37.60 (36.83)
	Residue	-	CrO	18.10 (17.81)
(3)	1st	155.9-313.3	-H_2O + L	47.0 (47.12)
	2nd	313.3-441.3	-CO + H_2	9.10 (9.06)
	3rd	441.3-616.1	- $C_3H_8NO_2$	27.62 (27.19)
	Residue		Mn	16.28 (16.59)
(4)	1st	155.9-218.6	-H_2O + 0.5Cl_2	11.62 (12.65)
	2nd	218.6-291.9	-0.5Cl_2 + HL	36.3 (37.06)
	3rd	291.9-537.3	-0.5Cl_2	9.1 (8.39)
	4th	537.3-670.6	-HL	29.74 (28.67)
	Residue	-	Fe	13.24 (13.22)
(6)	1st	182.2-310.9	-2H_2O + HL + 0.5 Cl_2	42.80 (41.72)
	2nd	310.9-514.7	-0.5 Cl_2	6.62 (7.68)
	3rd	530.9-706.1	-HL	27.0 (26.24)
	Residue	-	Cd	23.6 (24.35)

9.06 %) weight loss. The final degradation stage ended at 616.1 °C is attributing to the removal of a residual organic part in coordinator [$C_3H_8NO_2$] by 27.62 (calcd. 27.19 %) weight loss. The final residue is Mn atom by 16.28 (calcd. 16.59) weight percentage. The gradual degradation stages representing in TG and DTG curves for [FeCl($C_4H_{11}NO_3$)$_2$·2H_2O]·2Cl complex displays four degradation stages started at 155.9 °C and ended at 670.6 °C. The first degradation stage ended at 218.6 °C is attributing to the removal of H_2O + 0.5 Cl_2 by 11.62 (calcd. 12.65 %) weight loss. The second degradation stage ended at 291.9 °C may be attributed to 0.5 Cl_2 + HL by 36.3 (calcd. 37.06 %) weight loss. The third degradation stage ended at 537.3 °C may be attributed to 0.5 Cl_2 by 9.10 (calcd. 8.39 %) weight loss. The final degradation stage may be attributed to the removal of HL by 29.74 (calcd. 28.67 %) weight loss. The final residue recorded at 670.6 °C is attributing to Fe atom. The TG curves of [Cd($C_4H_{10}NO_3$)$_2$·2H_2O]·2Cl complex displays three degradation stages starting at 182.2 and ended at 706.1 °C. The first degradation stage ended at 310.9 °C may be attributed to the removal of 2H_2O + HL + 0.5 Cl_2 by 42.80 (calcd. 41.72 %) weight loss. The second degradation stage ended at 514.7 °C may be attributed to the removal of 0.5 Cl_2 by 6.62 (calcd. 7.68 %) weight loss. The final degradation stage ended at 706.1 °C may be attributed to the removal of an organic ligand (HL) by 27 (calcd. 26.24 %) weight loss. The final residue is found attributed to the Cd atom.

Molecular modeling of the ligand and its complexes: To give an insight about the structure proposed as well as the complexes stabilities, the geometrical molecular parameters are calculated (Table-5). Total energy, binding energy, isolated atomic energy, electronic energy, heat of formation and dipole moment are the calculated parameters. Fig. 4, displays the molecular modeling for the investigated complexes implementing hyperchem 5.1. A comparison between the bond length

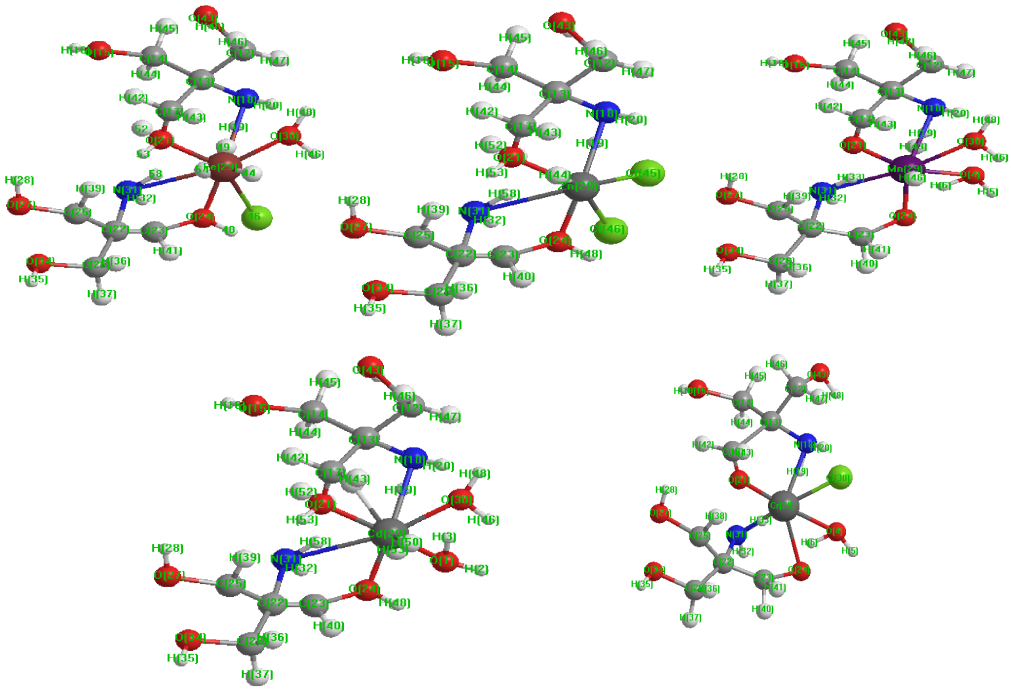

Fig. 4. Molecular modeling structure for all the solid metal complexes

TABLE-5
MOLECULAR MODELING PARAMETERS OF TRIZMA AND ITS METAL COMPLEXES

Assignment of the theoretical parameters	Theoretical data
$[C_4H_{11}NO_3]$	
Total energy	-38921.34244378 (kcal/mol)
Total energy	-62.0250996117 (a.u.)
Binding energy	-1692.5173007 (kcal/mol)
Isolated atomic energy	-37228.8251430 (kcal/mol)
Electronic energy	-176842.1674482 (kcal/mol)
Core–core interaction	137920.8250045 (kcal/mol)
Heat of formation	-144.1583007 (kcal/mol)
Gadient	0.0038051 (kcal/mol/Å)
Dipole moment	1.450 (Debyes)
$[CrCl(C_4H_{10}NO_3)_2(H_2O)]\cdot 2(H_2O)$	
Total energy	-97757.7414131 (kcal/mol)
Total energy	-155.786858013 (a.u.)
Binding energy	-3723.1008851 (kcal/mol)
Isolated atomic energy	- 94034.6405280 (kcal/mol)
Electronic energy	-693767.6819432 (kcal/mol)
Core-core interaction	596009.9405301 (kcal/mol)
Heat of formation	-442.8338851 (kcal/mol)
Gadient	0.0009960 (kcal/mol/Å)
Dipole moment	4.668 (Debyes)
$[FeCl(C_4H_{11}NO_3)_2H_2O]\cdot 2Cl$	
Total energy	-104879.6295845 (kcal/mol)
Total energy	-167.136298278 (a.u.)
Binding energy	-3884.3430605 (kcal/mol)
Isolated atomic energy	-100995.2805240 (kcal/mol)
Electronic energy	-760187.1620731 (kcal/mol)
Core-core interaction	655307.5384885 (kcal/mol)
Heat of formation	-630.3450605 (kcal/mol)
Gadient	0.0009127 (kcal/mol/Å)
Dipole moment	8.539 (Debyes)
$[Mn(C_4H_{10}NO_3)_2\cdot 2H_2O]$	
Total energy	-100798.6754957 (kcal/mol)
Total energy	-160.632894340 (a.u.)
Binding energy	-3805.6084607 (kcal/mol)
Isolated atomic energy	-96993.0670350 (kcal/mol)
Electronic energy	-718970.8474336 (kcal/mol)
Core-core interaction	618172.1719379 (kcal/mol)
Heat of formation	-469.9704607 (kcal/mol)
Gadient	0.0008185 (kcal/mol/Å)
Dipole moment	74.068 (Debyes)
$[ZnCl_2(C_4H_{11}NO_3)]$	
Total energy	-93137.7499660 (kcal/mol)
Total energy	-148.424433910 (a.u.)
Binding energy	-3511.1042830 (kcal/mol)
Isolated atomic energy	-89626.6456830 (kcal/mol)
Electronic energy	-628799.4102527 (kcal/mol)
Core-core interaction	535661.6602868 (kcal/mol)
Heat of formation	-325.2362830 (kcal/mol)
Gadient	2.4421699 (kcal/mol/Å)
Dipole moment	13.751 (Debyes)
$[Cd(C_4H_{11}NO_3)_2\cdot 2(H_2O)]\cdot 2Cl$	
Total energy	-92883.9384505 (kcal/mol)
Total energy	-148.019959564 (a.u.)
Binding energy	-3371.1449245 (kcal/mol)
Isolated atomic energy	-89512.7935260 (kcal/mol)
Electronic energy	-645747.8472836 (kcal/mol)
Core-core interaction	552863.9088332 (kcal/mol)
Heat of formation	-189.7269245 (kcal/mol)
Gadient	19.4210526(kcal/mol/Å)
Dipole moment	17.686 (Debyes)

of the significant groups in the ligand with the same in complexes is deliberately observed. The bond length data of ligand indicates that, the N-H is coincided with the x-ray measured lengths while, O-H bond is shorter than those recorded in x-ray. Moreover, it is clear that O(1)-H(14) is longer than other O-H bonds which may be attributed to their involvement in intramolecular H-bonding. The bond length data around the Cr atom indicate that, Cr(III) has a distorted octahedral structure. This is due to the presence of two bond types (-NH_2 and -O) with Cr(III), where the O(21) and O(24) have a longer bond length referring to their covalent attachment with the central atom. Also, there is a difference between Cr-N and Cr-Cl (0.22 Å). The bond length data of Fe(III) complex show a high distortion from the regular octahedral structure values, where the axial Fe(29)-Cl(46) is longer than the equatorial Fe(29)-OH_2(30) by 0.3 Å. While, the axial O(21)-Fe(29) is longer than other Fe-O bonds which reveals the elongation of z-axis in octahedral structure. The Mn complex bond length data is more symmetric than other complexes. The data display a little difference between Mn-O bond with ligand where O(21)-Mn(29) is longer the others by 0.04 Å which may be attributed to ruling out of O(21) in involvement in H-bond while the others are. The bond length data of Zn(II) complex is the most symmetrical complexes where as the difference between the same atoms bond length is ranged from 0.0002 to 0.01 Å despite the difference in between in the bonds. The Cd(II) complex is also showing smaller distortion in bond length where difference between atoms of the same type is ranged from 0.0001 to 0.001 Å despite the difference between different bonds. From the calculations of the internal energy of all compounds, the relative stability can be observed. From the data tabulated in Table-5, the stability of the complexes can be arranged as fellow: Cr(III) complex is stabilized than Fe(III) as well as, the Cd(II) complex is the highly stable in between the bivalent ion complexes.

Biological activity

DNA degradation effect: The DNA degradation behavior under the effect of the ligand and their complexes is examined. A comparison reflects the completely difference in the results obtained after mixing the calf thymus DNA with the ligand and with each complex. The results shown in the photos (Fig. 5) that, the ligand and DMSO did not degrade the DNA and the DNA migration was close to the top of the gel. Whereas, all the complexes degraded the DNA almost completely in comparing with their original ligand. This behavior is illustrated referring to the direct contact of such slim complexes with the DNA which able to degrade it. The absence of the crudeness surround the central atoms facilitate the direct interaction.

Antimicrobial activity: The ligand and its metal complexes were tested against *Bacillus sp*. as gram positive and *Klebsiella* sp. and *Proteus* sp. as gram negative bacteria for their antibacterial activities (Table-6) using the disk diffusion sensitivity testing method. Generally speaking the antimicrobial activities were scored according to the Clinical Laboratory and Standards Institute (CLSI) and classified into three categories: R: resistant microbe (the diameter of the zone of inhibition equal 1.4 cm or less), I: intermediate sensitive microbe (the diameter of the zone of inhibition ranges from 1.5-1.7 cm) and

Fig. 5. Electrophoretic mobility of Calf thymus DNA treated with H_3AHMP (lane 1), ligand with DNA (lane 2), ligand with DMSO (lane 3), Fe complex (lane 4), Mn complex (lane 5), Cr complex (lane 6), Cd complex and (lane 7), for Zn complex

TABLE 6
VALUES OF ZONE INHIBITION OF MICROORGANISMS FOR TRIZMA AND ITS METAL COMPLEXES

Compound	Zone of inhibition (mm)		
	Gram (+) bacteria	Gram (–) bacteria	
	Bacillus subtilis	*Klebsiella sp.*	*Proteus sp.*
1	1.0 R	0.0 R	0.0R
2	0.0 R	0.0 R	0.0R
3	0.0 R	0.0 R	0.0R
4	0.0 R	0.0 R	0.0R
5	1.5 I	1.0 I	1.1 I
6	2.0 S	2.9 S	1.3 L

R: resistant, I: intermediate sensitivity and S; Susceptible

S: sensitive microbe to the tested agent (the diameter of the zone of inhibition is more than 1.8 cm. The Cd(II) and Zn(II) complexes showed bacteriostatic activity, meaning the complex initially suppressed the growth of the target microbe in the immediate contact vicinity for about 24 h, then the complex degrades fast and the inhibited microbes resume growth in the same vicinity. This is indicated by the zones of inhibition diameter. Whereas, the other metal complexes were non effective against all microorganisms. The negative results can be attributed either to the in ability of the complexes to diffuse into the Gram-negative or the Gram-positive bacterium and hence unable to interfere with its biological activity or they can diffuse and inactivated by unknown cellular mechanism by the bacterium.

REFERENCES

1. R.G. Bates, C.A. Vega and D.R. White, *Anal. Chem.*, **50**, 1295 (1978).
2. G.G. Nahas, *N.Y. Acad. Sci.*, **92**, 333 (1961).
3. G.G. Nahas, *Pharm. Rev.*, **14**, 447 (1962).
4. G.G. Nahas, *Science*, **129**, 782 (1959).
5. F. Manfredi, H.O. Seiker, A.P. Spoto and H.A. Saltzman, *JAMA*, **173**, 999 (1960).
6. J.A. Frump, *Chem. Rev.*, **71**, 483 (1971).
7. W.N. McFarland and K.S. Norris, *Calif. Fish Game*, **44**, 291 (1958).
8. D.B. Hall, R.E. Holmlin and J.K. Barton, *Nature*, **382**, 731 (1996).
9. B. Lippert, *Coord. Chem. Rev.*, **200-202**, 487 (2000).
10. C. Liu, M. Wang, T. Zhang and H. Sun, *Coord. Chem. Rev.*, **248**, 147 (2004).
11. K. Ghosh, P. Kumar, N. Tyagi, U.P. Singh and N. Goel, *Inorg. Chem. Commun.*, **14**, 489 (2011).
12. Y.P. Li and P. Yang, *Inorg. Chem. Commun.*, **14**, 545 (2011).
13. X.W. Li, Y. Yu, Y.T. Li, Z.Y. Wu and C.W. Yan, *Inorg. Chim. Acta*, **367**, 64 (2011).
14. H. Liu, X. Shi, M. Xu, Z. Li, L. Huang, D. Bai and Z. Zeng, *Eur. J. Med. Chem.*, **46**, 1638 (2011).
15. (a) B.B. Lohray, V.B. Lohray, B.K. Srivastava, P. Kapadnis and P.P. Pandya, *Bioorg. Med. Chem.*, **12**, 4557 (2004); (b) D.E. King, R. Malone and S.H. Lilley, *Am. Fam. Physician*, **61**, 2741 (2000); (c) C.H. Gross, J.D. Parsons, T.H. Grossman, P.S. Charifson, S. Bellon, J. Jernee, M. Dwyer, S.P. Chambers, W. Markland, M. Botfield and S.A. Raybuck, *Antimicrob. Agents Chemother.*, **47**, 1037 (2003).
16. J.A. Cowan, *Chem. Rev.*, **98**, 1067 (1998).
17. A. Sreedhara and J.A. Cowan, *J. Biol. Inorg. Chem.*, **6**, 337 (2001).
18. B. Meunier, *Chem. Rev.*, **92**, 1411 (1992).
19. E.L. Hegg and J.N. Burstyn, *Coord. Chem. Rev.*, **173**, 133 (1998).
20. S.D. Dhmwad, K.B. Gudasi and T.R. Goudar, *Indian J. Chem.*, **33A**, 320 (1994).
21. A.I. Vogel, Text Book of Quantitative Inorganic Analysis Longman, London, p. 505 (1986).
22. N.L. Allinger, *J. Am. Chem. Soc.*, **99**, 8127 (1977).
23. Hyper Chem. Version 7.51 Hyper cube, INC.
24. F. Hartl, P. Barbaro, I.M. Bell, R.J.H. Clark, T.L. Snoeck and A. Vlcek Jr., *J. Inorg. Chim. Acta*, **252**, 157 (1996).
25. T.B. Karpishin, M.S. Gebhard, E.I. Solomon and K.N. Raymond, *J. Am. Chem. Soc.*, **113**, 2977 (1991).
26. I. Michaud-Soret, K.K. Andersson, L. Que and J. Haavik, *J. Biochem.*, **34**, 5504 (1995).
27. A.B.P. Lever, Inorganic Electronic Spectroscopy, Elsevier, Amsterdam, edn 1 (1968).
28. F.A. Cotton, G. Wilkinson, C.A. Murillo and M. Bochmann, Advanced Inorganic Chemistry, Wiley, New York, edn 6 (1999).
29. S.S. Kandil, G.B. El-Hefnawy and E.A. Baker, *Thermochim. Acta*, **414**, 105 (2004).